REPORT DOCUMENTATION PAGE

Form Approved
OMB No. 0704-0188

1. REPORT DATE *(DD-MM-YYYY)*	**2. REPORT TYPE**	**3. DATES COVERED** *(From - To)*
15-02-2006	Journal Article PREPRINT	2005-2006

4. TITLE AND SUBTITLE

Fast Surface Temperature Measurement of Teflon Propellant in Pulsed Ablative Discharges Using HgCdTe Photovoltaic Cells

(PREPRINT)

5a. CONTRACT NUMBER

5b. GRANT NUMBER

5c. PROGRAM ELEMENT NUMBER

6. AUTHOR(S)

Erik L. Antonsen, Rodney L. Burton, *Garrett A. Reed, †Gregory G. Spanjers

5d. PROJECT NUMBER

5e. TASK NUMBER

5f. WORK UNIT NUMBER

7. PERFORMING ORGANIZATION NAME(S) AND ADDRESS(ES) AND ADDRESS(ES)

University of Illinois
Urbana-Champaign, IL 61801

*ERC Inc.
10 E. Saturn Blvd
Edwards AFB, CA 93524

8. PERFORMING ORGANIZATION REPORT NUMBER

9. SPONSORING / MONITORING AGENCY NAME(S) AND ADDRESS(ES)

†Air Force Research Laboratory
Space Vehicles
3550 Aberdeen Ave SE
Kirtland AFB, NM 87117-5776

10. SPONSOR/MONITOR'S ACRONYM(S)

11. SPONSOR/MONITOR'S REPORT NUMBER(S)

AFRL-VS-PS-JA-2006-1007

12. DISTRIBUTION / AVAILABILITY STATEMENT

Approved for public release; distribution is unlimited. (Clearance # VS06-0068)

13. SUPPLEMENTARY NOTES

Submitted for publication in Review of Scientific Instruments

Government Purpose Rights

14. ABSTRACT

High speed Mercury Cadmium Telluride photovoltaic detectors sensitive to infrared emission are investigated as a means of measuring real-time surface temperature on a micro-second timeframe pulsed ablative discharge with Teflon™ as the ablated material. Analysis is used to derive a governing equation for detector output voltage for materials with wavelength dependent emissivity. The detector output voltage is experimentally calibrated against thermocouples embedded in heated Teflon. Experimental calibration is performed with Teflon that has been exposed to ~200 pulsed discharges and non plasma-exposed Teflon. These are compared to theoretical predictions to analyze emissivity differences between plasma-exposed and non plasma-exposed Teflon. The diagnostic capability is evaluated with measurements of surface temperature from the Teflon propellant of electric micro-Pulsed Plasma Thrusters. During the capacitive discharge, there is insufficient information to claim that the surface temperature is accurately measured. However, immediately following the discharge, the post-pulse cooling curve is measured. The statistical spread of post-pulse surface temperature from shot-to-shot, most likely due to arc constriction and localization, is investigated to determine an operational envelope for post-pulse temperature and mass ablation. This information is useful for determining post-pulse ablation contributions to mass loss as well as evaluation of theoretical discharge models currently under development.

15. SUBJECT TERMS

Space Vehicles; Surface Temperature; Teflon™; Photovoltaic Detectors; Detector Output Voltage; Emissivity; Plasma; Theoretical Discharge Models

16. SECURITY CLASSIFICATION OF:			**17. LIMITATION OF ABSTRACT**	**18. NUMBER OF PAGES**	**19a. NAME OF RESPONSIBLE PERSON**
a. REPORT	**b. ABSTRACT**	**c. THIS PAGE**			Gregory G. Spanjers
Unclassified	Unclassified	Unclassified	Unlimited	39	**19b. TELEPHONE NUMBER** *(include area code)* 505-846-9330

Fast Surface Temperature Measurement of Teflon Propellant in Pulsed Ablative Discharges Using HgCdTe Photovoltaic Cells.

Erik L. Antonsen and Rodney L. Burton
University of Illinois at Urbana-Champaign, IL 61801
eantonse@uiuc.edu

Garrett A. Reed
ERC Inc., Edwards AFB, CA 93524

Gregory G. Spanjers
Air Force Research Laboratory, Space Vehicles Directorate, Kirtland AFB, NM 87117

ABSTRACT

High speed Mercury Cadmium Telluride photovoltaic detectors sensitive to infrared emission are investigated as a means of measuring real-time surface temperature on a micro-second timeframe pulsed ablative discharge with Teflon™ as the ablated material. Analysis is used to derive a governing equation for detector output voltage for materials with wavelength dependent emissivity. The detector output voltage is experimentally calibrated against thermocouples embedded in heated Teflon. Experimental calibration is performed with Teflon that has been exposed to ~200 pulsed discharges and non plasma-exposed Teflon. These are compared to theoretical predictions to analyze emissivity differences between plasma-exposed and non plasma-exposed Teflon. The diagnostic capability is evaluated with measurements of surface temperature from the Teflon propellant of electric micro-Pulsed Plasma Thrusters. During the capacitive discharge, there is insufficient information to claim that the surface temperature is accurately measured. However, immediately following the discharge, the post-pulse cooling curve is measured. The statistical spread of post-pulse surface temperature from shot-to-shot, most likely due to arc constriction and localization, is investigated to determine an operational envelope for post-pulse temperature and mass ablation. This information is useful for determining post-pulse ablation contributions to mass loss as well as evaluation of theoretical discharge models currently under development.

1. INTRODUCTION

Propellant surface temperature measurements are critical to further development of the micro-Pulsed Plasma Thruster (micro-PPT).[1] A micro-PPT is a spacecraft propulsion device that uses a pulsed (~20 μs) electrical surface discharge across the face of a solid Teflon™ propellant. The discharge ablates a small amount of material (~4 μg), ionizes it to plasma, and electromagnetically accelerates it to create thrust. Following the pulsed discharge another mass (~1.2 ug) of neutral vapor and particulates is emitted from the device. The surface temperature measurements are needed to better understand the conversion from solid propellant to plasma accelerant and characterize the effects of late-time neutral vapor generation to thruster performance. In addition, post-pulse temperature measurements are needed to develop and verify models of interaction between the spacecraft and the exhaust.

Analysis of the post-pulse mass ejected from PPTs has typically been performed with interferometry sensitive to neutral vapor after the pulse.[2] With the development of the micro-PPT, the low energies typical of the discharge have limited the neutral density to levels below the sensitivity threshold of laser interferometers. A Herriott Cell was used to augment the resolution of these interferometers, but post-pulse neutral densities were still unmeasurable.[3] An alternative method of investigation is proposed to attempt a direct measurement of the propellant surface, since the equilibrium vapor pressure curve for Teflon is well known.[1,4]

Direct measurements of the propellant surface temperature can be achieved using photovoltaic cells. Research in the fracture dynamics community relies heavily on infrared photovoltaic detectors to characterize temperature rise near the tips of fast-propagating cracks in solid materials.[5,6,7] The time-frame under observation for these experiments is similar to timeframes during which a micro-PPT discharge is observed. It is a claim of this paper that real-time propellant surface temperature measurements can be accomplished using the similar techniques. The relationship between surface temperature and Teflon vapor pressure is well known at high temperatures. Through this relationship, surface temperature (T_S) governs ablation rate in these thrusters and becomes critical in calculation of total mass loss, available charge carriers, and late-time ablation. These extend the influence of T_S to plasma resistivity, ionization fraction, current density, and the feedback process of ablation from arc radiation and particle convection. Surface temperature is the defining parameter for thruster operation and analysis, which until now has been un-measurable in real-time for these thrusters.

This paper is directed towards validating the use of the photovoltaic detectors in high-speed, pulsed plasma-wall interaction applications. An inherent problem for performing this measurement is the wavelength dependent emissivity of polymers used for pulsed discharge applications. Teflon has a wavelength dependent emissivity and is used for a number of applications including electric rocket propulsion[1,8,9] and plasma opening switches.[10,11] Teflon is also an ideal candidate material for this investigation. Vaporization from the surface of Teflon generally leaves a smooth surface with minimal changes in emissivity.

Section 2 describes the apparatus and experimental approach for calibration of photodiode voltages from heated Teflon along with diagnostic application to the thruster face. Emissive differences between plasma-exposed and non-plasma-exposed Teflon are addressed experimentally. In Section 3, a theoretical estimate of the expected detector output for heated Teflon is derived. Data from infrared spectroscopy is used to estimate wavelength dependent emissivity. Theoretical prediction helps assess background emissivity differences between plasma-exposed and non-plasma-exposed Teflon samples for calibration. Additionally, a short review of the Keidar-Boyd Model[12-14] predictions for surface temperature is presented. In Section 4, the diagnostic capability is demonstrated with measurements of surface temperature, comparison with Keidar-Boyd Model predictions, and discussion of the limitations of the diagnostic.

2. APPARATUS

2.1 Plasma Source

The plasma source is a micro-Pulsed Plasma Thruster[1] with an outer electrode diameter of 6.35 mm, an inner electrode diameter of 1.64 mm, an outer Teflon diameter of 5.46 mm, and RLC discharge energy of 4.35 J. The source is operated in single pulse mode to minimize steady-state temperature gain throughout the thruster body and propellant.

2.2 Detector and Optics

The HgCdTe photovoltaic detector is chosen for its broad range of responsivity over 2-12 μm wavelengths and high speed response. A linear array of 4 detectors made by Fermionics[15] has DC to 10 MHz bandwidth for an active area of 80 μm x 80 μm square and a pitch of 20 μm between detectors. Peak responsivity (R_p) is 8.2 A/W with a detector rise time ~40 ns. Figure 1 shows the 4 detector array superimposed over the thruster face to scale for assessment of the spatial resolution.

The optics for infrared detection use a 15.2 cm diameter gold coated concave spherical mirror with a 30.5 cm focal length and a 50 mm diameter gold coated flat mirror. A distance of 61 cm from the spherical mirror to both the target and the detector is maintained. The 50 mm flat mirror is placed 36 cm from the spherical mirror to complete the Newtonian telescope. Figure 2 shows a schematic of this layout.

Targeting for both the calibration apparatus and thruster face during experimental testing is performed using crossed tungsten wires of 80 μm diameter. Current up to 1.2 A is run through each wire to induce thermal emission. The signal is maximized by moving the detector array forward and backward to locate the signal maximum corresponding to the focal point of the telescope. The Newtonian telescope is then used to target first horizontally and then vertically with the two crossed wires.

2.3 Calibration Assembly

To calibrate detector voltage output with actual heated Teflon temperature, a 3.175 mm thick sheet of Teflon is sandwiched between two copper plates with optical access holes 5.38 mm in diameter in both copper plates. Three type K thermocouples are drilled into the sides of the Teflon sheet and embedded close to the point where the IR detector is imaged. The Newtonian telescope images the detectors at 1:1 magnification onto the Teflon surface. Figure 3 shows a photo of the front of the calibration apparatus with thermocouples embedded (left) and a photo of the apparatus with the back removed highlighting the thermocouple shadows embedded in the Teflon sample (right). This illustrates the relative location of the thermocouple measurement and the detector focal point. The baseplate of the apparatus is seated on a Micropyretics Heaters International (MHI) hotplate. Two copper plates are hinged to form a triangle of reflective metal that sits over the apparatus and reflects heat back at the calibration apparatus. Optical access for the Newtonian telescope is provided through a 25.4 mm conflat viewport made of Zinc Selenide (ZnSe). Heat is transferred through the baseplate to the front copper plate which then heats the front side of the Teflon. Data from the thermocouples and detectors are recorded by a data logger at 1 or 2 second intervals. A typical calibration takes about 10 hours. A slow heating scheme is used to increase accuracy by reducing transient thermal effects.

During pulsed discharge, problems with Teflon surface charring[12] can occur that affect material emissivity. There also exists the possibility that a clean, plasma-exposed surface will exhibit different emissive characteristics than a virgin (non plasma-exposed)

Teflon surface. A demonstration of the effects of the plasma on a plasma-exposed surface is necessary to determine if the exposure affects the emissivity of Teflon propellant, and therefore the calibration curve. A thruster breadboard with copper electrodes and a Teflon sheet underneath is used to expose Teflon suitable for calibration tests to plasma conditions experienced by the micro-PPT surface to determine if there are significant changes to IR emissivity. Samples have been exposed to 4.35 J discharges for pulse numbers ranging from 100 up to 1500 pulse exposures. These are compared with non plasma-exposed Teflon samples to characterize changes in IR emissivity that may occur with plasma exposure.

2.4 Quantifying Plasma Effects

To experimentally characterize the emission from the plasma and neutral vapor above the fuel face, IR measurements are taken with the detector optical cone targeted to a point in front of the central electrode and traversing across the exit plane of the thruster. The view cone in this orientation does not intersect the surface of the micro-PPT. Figure 4a shows the cone apex targeted schematically to illustrate this configuration. Figure 4b shows the apex of the optical cone intersecting the propellant face, the configuration used when measuring the surface temperature of the propellant. By measuring emission from the plasma and neutral vapors without a heated background, the emissive contribution of the plasma and neutral vapor is characterized. If the plume contribution ends when the current pulse ends, then the surface can be measured after that time without emissive interference from the exhaust. To characterize this, measurements across the fuel face are made with the focal point of the optics located at 1 mm, 3 mm, 5 mm, and 7 mm in

from of the fuel face. When these measurements are compared to fuel face measurements, an assessment concerning optimal viewing time during the pulse is made. Repeated tests show that after the current reversal stops, there is no measurable detector signal. These results are discussed below, but here it is sufficient to state that after the current pulse ends, plasma and vapor emission contribution also ends and a clear surface measurement can be obtained.

3. THEORY

3.1 Teflon Emission

The distribution of radiation emitted from a body depends on temperature and is described by the Plank function[16]

$$P_E = \frac{C_1}{\lambda^5\left(e^{\frac{C_2}{\lambda T}} - 1\right)} \qquad (1)$$

where C1 is 3.742×10^8 W-μm^4/m^2, C2 is 1.439×10^4 μm-K, λ is the radiation wavelength (μm), and T is the material temperature (K). This equation yields spectral emissive power for a black body. For Teflon emission we derive an expected detector output from calibration with a Teflon sample using data from transmissive spectroscopy as a starting estimate.[17] For any material,[18]

$$\rho + \alpha + \tau = 1 \qquad (2)$$

where ρ is the reflectivity, α is the absorptivity, and τ is the transmissivity. Areas of high absorption correspond to areas of high emission since energy absorption equals energy emission from the stretching and bending modes of the C-F bonds in the Teflon

molecules. The reflectivity of Teflon in the wavelengths of interest is unknown, but from Eqn. 2 it is assumed that material reflectivity decreases the amount of total emission. Therefore, if the reflectivity is omitted in a prediction of detector response, an overprediction of the total emission is expected. This expected overprediction in noted in the final estimates. Eliminating reflectivity and setting absorptivity equal to emissivity (ε) converts Eqn. 2 to

$$\varepsilon = 1 - \tau \tag{3}$$

allowing an estimate of the wavelength dependent emissivity for Teflon. An emissive peak of unity at 8.4 μm is the chief emissive source[4,17] along with an overtone at 4.4 mm of ~0.5 due to superposition of the stretching and bending modes present in the C-F bonds. Figure 5a shows an estimate of Teflon emissivity. Using this estimate, an expected spectral emissive power for the 2-12 μm range is calculated.

A first order determination of the expected total emission and response is obtained by combining the Plank distribution for Teflon with the wavelength dependent detector responsivity and integrating over the range of wavelengths (2-12 μm). This gives an expected detector current output calculated by

$$I_E = \int_\lambda D^* R_p \varepsilon_\lambda P_E d\lambda \tag{4}$$

where D* is the normalized wavelength dependent responsivity, R_p is the peak responsivity, ε_λ is the wavelength dependent emissivity, and P_E is the spectral emissive

power calculated by Eqn.1. Equation 1 yields the total power emitted from the specimen, however, only a fraction of that power is observed by the detector. Assuming 1:1 imaging, with a detector view angle limited by the flat mirror (50.8 mm DIA) the half angle of the viewable cone is 3.05° on average. The angular area of a hemisphere is 2π, and the angular area of a small circle of angular radius θ is given by[19]

$$\Omega_c = 2\pi(1-\cos\theta) \tag{5}$$

The ratio of the circle solid angle to the hemispherical solid angle is simply $(1-\cos\theta)$, which is the ratio of the power received to the power emitted.

The effect of the optics on total intensity is included. The Newtonian telescope uses two gold mirrors with a reflectivity of 0.99 in the relevant wavelength range. Additionally, since the calibration is performed at vacuum, the transmissivity of the viewport material is included. The optical viewport on the vacuum chamber is ZnSe, chosen to maximize the total transmission in the LWIR (τ=0.7 from 2-12 mm). The optical response is defined as a constant, k_o, which is the multiplied value of all mirror reflectivities and window transmissivities. Multiplication of the ultimate detector output by this constant corrects for losses in the optical system.

Since the optics provide an imaging system, the detector is operated with a 1:1 magnification of the detector element onto the surface of the specimen. Only emission coming from within the viewable cone (the apex of which is the detector image) can be sensed. The detector active area limits the total number of photons collected from the

optics, therefore the active area, A, is included. Each detector is a square with 80 μm to a side for an area of 6.4×10^{-9} m^2.

Finally, the amplifier has a transimpedance factor (V_{out}/I_{in}), of 20000 V/A. This is the gain of the pre-amplifier and is denoted here as G. The combined end result for estimating detector voltage out is

$$V = k_o GA(1-\cos\theta)\int_{\lambda} D^* R_P \varepsilon_\lambda P_e d\lambda \qquad (6)$$

Using Eqn. 6 and noting the omission of Teflon reflectivity in the estimation of the emissivity, a calculation for the output voltage from this detector measuring heated Teflon can be made. Since an overprediction is expected for the Teflon response, an experimental calibration curve is obtained to demonstrate the deleterious effects of the assumptions up to this point. These results are discussed in section 4.

Comparison of the predictions from Eqn. 6 with experimental calibration requires the estimate of the emissivity shown in Figure 5a. To determine if calibration results are valid, the heating and cooling curves for detector voltage out vs. surface temperature must match. If the thermocouples are measuring close to the location of the emission measurement, and there are no changes to surface condition during the test, both curves will demonstrate the same emission. Reasons why the two curves might not match include Teflon expansion out of the viewing hole (which causes a change in the optical path), targeting errors, material depositing on the surface of the Teflon causing a change in emissivity, or possibly a permanent change in emissivity due to thermal cycling of the

Teflon. For the experimental setup used here, the heating and cooling curves match and are used to determine a useful estimate of emissivity. With all other terms in Eqn. 6 known as well as the major emissive structures, the emissivity background is adjusted to match the experimental calibration curve discussed in Section 4.1. This allows calculated extrapolation of temperatures beyond the physical calibration limit of 750 K.

3.2 Vapor Optical Thickness

The experimental setup used here cannot measure surface temperature during current reversal due to emission encountered from plasma and neutral vapor situated above the Teflon face. As the surface is heated during the arc, these two regions exist at high temperatures and may be capable of emission within the measurement range of the detectors. Determination of whether surface emission may be viewed is dependent upon the optical thickness of the plasma and neutral vapor. Calculation of wavelength dependent optical thickness is beyond the scope of this inquiry, but a more simple optical thickness calculation is possible.

Presence of plasma may hinder photon collection by re-absorption of the radiated photons. The magnitude of this effect is estimated by calculating the optical thickness as the non-dimensional ratio of the plasma scale length to the characteristic length of photon motion prior to reabsorption.

$$\tau = \frac{l_p}{l_\gamma} \tag{7}$$

Therefore an optical depth much less than 1 indicates a high likelihood for photons generated within the plasma to reach the edge without reabsorption and be available for collection by the diagnostic optics.

The plasma optical thickness for a doppler broadened line[20] is given by (CGS units)

$$\tau = 1.76 \times 10^{-13} \lambda \left(\frac{Mc^2}{kT_e} \right)^{\frac{1}{2}} N_e l_p \qquad (8)$$

where M is the atomic mass (averaged to 16.7 AMU or 2.77×10^{-23} gm), c is the speed of light, k is the Boltzmann constant, T_e is the electron temperature, N_e is the number density, and l_p is the plasma depth. Inserting typical values for a micro-PPT ($N_e = 1 \times 10^{16}$ cm^{-3}, T_e = 11500 K (1 eV), l = 0.635 cm (using the thruster diameter), 6 μm wavelength), gives $\tau = 8 \times 10^4$. This suggests that the plasma is optically thick. Emission from the Teflon surface is likely to be reabsorbed by the plasma and not reach the detector. The optical thickness of the plasma may limit the usefulness of the diagnostic to after the conclusion of the plasma discharge. Note that this analysis for optical depth presumes that the transitions in the solid Teflon at the propellant face will be very close to the line transitions in the plasma. If these transitions are at significantly different wavelengths, the plasma may be more optically thin than indicated by these calculations.

There is an experimental means of determining whether the surface emission can be independently collected during and after the pulse. Both plasma and neutral vapor emission can be accounted for experimentally by measuring the total emission in the viewable cone in an area where they are present. By targeting across the surface of the thruster over the central electrode, the plasma and vapor contribution can be assessed.

This method characterizes the gaseous emission throughout the pulse and is described in Section 2.4.

3.4 Keidar-Boyd Model

The Keidar-Boyd model is an end-to-end (plasma generation to plume far field) model specifically addressing the geometry of the microPPT with regards to thruster performance and spacecraft contamination issues. Three models are employed to investigate the complete discharge of the micro-PPT. The first model is a first-order ablation model that characterizes Teflon loss to the arc. The second is a description of the Teflon transition through neutral vapor to plasma in several sublayers. Finally, there is a Particle-in-Cell (PIC) description of the plume to far field. These models use a fluid description of the electrons, a direct simulation Monte Carlo (DSMC) model of the neutrals, and a PIC description of the ions. The ablation and plasma generation models provide boundary conditions for the plasma plume model.[12-14] This allows for a consistent description of the plasma flow from the Teflon surface into the near plume. Because of this fact, the plume properties depend very heavily on the upstream conditions including surface temperature. The Keidar-Boyd model considers arc constriction in calculation of surface temperature by two means of heating. When the area being heated is directly under the constriction, heating is performed by a mixture of particle convection and radiation to the surface. In cases where the area being heated is far from the constriction (i.e. opposite side of the thruster face) the dominant heating mechanism is radiation while particle convection is neglected. Predictions of surface temperature from this model are compared to experimental results below.

4. RESULTS AND DISCUSSION

4.1 Calibration Results

Figure 6 shows the calibration data for both non plasma-exposed and plasma-exposed Teflon along with the theoretical detector output using the emissivity estimate from Eqn. 6. The most significant result is that the small degree of disagreement between virgin Teflon and plasma exposed Teflon can be explained completely through a small change in background emissivity. Figure 5 a. and b. show the difference in background emissivity required to match the observed difference in calibration. For the non plasma-exposed case, the background emissivity is set at 0.04. Keeping the major emissive structures constant and reducing the background emissivity to 0.01 results in good agreement between the experimental data for plasma exposed Teflon and the modeled calibration. Because the top layers of Teflon in the thruster undergo thermal cycling from repetitive pulsing, changes in the crystalline structure result in a slightly different emissivity than non plasma-exposed Teflon. The small degree of disagreement between virgin and plasma exposed Teflon calibrations suggests that there is very little emissive contribution that cannot be traced to the C-F stretching mode.

Representative data points from experimental calibrations are shown along with a parabolic fit of those data points. These are also compared with a theoretical prediction from Eqn 6 (which lies directly on the parabolic fit). The fit for the plasma-exposed calibration curve is

$$V = 2.87 * 10^{-5} T^2 \qquad (9)$$

Beyond the peak measured temperature of 750 K, the voltage is calculated using Eqn. 6. For these experiments, the calibration sample is conditioned with ~100 pulses before testing. The plasma-exposed calibration curve is used to translate detector voltages into the temperature domain for measurements from thruster propellant faces.

The experimental calibration limit of 750 K is due to solid Teflon deformation at higher temperatures. This has the effect of changing the optical path and invalidating the calibration. Therefore calibration data above this temperature is calculated using Eqn. 6. While it is possible that the calibration could change at these temperatures, there is no evidence to suggest a change in the major emissive structures at 8.4 and 4.4 μm since these are the result of vibrational modes present in the polytetrafluoroethylene monomers even after the polymer has completely unzipped.

The uncertainties in Figure 6 are calculated by a root-mean square standard deviation of 5 calibration tests combined with the ±0.3 mV resolution of the detector. Also shown are temperature uncertainties using the same method based on the thermocouple uncertainty. For the K-type thermocouples used, the uncertainty is ±2.2 K or .0075*T, whichever is larger. Another term is introduced for ±8 K representing the temperature difference between the embedded thermocouple location and the center of the calibration target where emission measurements are made. This value is obtained from experimental data and ANSYS predictions.

4.2 Plume Emissive Contribution

Measurements of the plume emission alone determine the contribution of plasma emission during the discharge to the total signal measured. By noting where in time the

plume contribution ends, a timeframe for possible surface viewing is determined. Measurements taken at 1, 3, 5, and 7 mm away from the propellant face show that plume contribution drops to zero throughout the discharge by 5 mm from the fuel face indicating that the plume expansion at that point has limited the total emission that the detectors can sense. Figure 7 shows an uncalibrated comparison of surface measurement with a plume measurement at 1 mm distance from the propellant surface. Cessation of signal from the plume occurs at or before the end of the current pulse. From this data we define acceptable surface temperature data as that which occurs after the current pulse is extinguished. In the data presented below, surface temperature data begins at 26 μs after initiation of the discharge.

4.3 Surface Temperature Measurements

Figure 8 shows 14 distinct data traces taken while targeting the thruster propellant face. Initial post-pulse temperatures (t=26 μs) observed range between 600 and 850 K. Cooling rates appear roughly constant from pulse to pulse. These data have been filtered digitally using a low-pass filter cutting off frequencies above 300 kHz. There is a small amount of electrical noise at about 55 μs not removed by the filter present in each pulse. This defines an operating envelope of surface temperatures that can be explained by differences in arc spoking characteristics between pulses.[14]

The spatial resolution of the detector in these experiments is limited to the detector size as imaged on the propellant face. Since this is 1:1, the detector only sees 80 x 80 μm^2 of surface area. This is a small fraction of the total propellant area exposed to

the effects of the arc. Figure 9 shows DICAM images of a micro-PPT firing at a.) 2.3 J, b.) 5.55 J, and c.) 6.73 J. These firings used a 0.417 μF capacitor with the central electrode as the cathode. The discharge voltages are then a.) 3300 V, b.) 5200 V, and c.) 5700 V. The trend observed is that at low discharge voltages, there is a greater likelihood of a symmetrical discharge across the propellant face. At the higher energies the emission suggests that anode spots form on the outer electrode which indicates the possibility of current constriction across portions of the propellant face. If the detector measures directly underneath an arc constriction, the post-pulse surface temperature is expected to be higher than is the detector measures a portion of the propellant that is distant from the arc constriction. Using the voltage and temperature uncertainties discussed above, individual pulse uncertainties are compared for two of the extreme cases in post-pulse temperature measured. Figure 10 shows comparison of a.) the highest temperature cooling curve from the data set (Pulse 20) compared with the surface temperature predicted for an area covered by the arc constriction. Part b.) shows a comparison of the lowest temperature cooling curve from the data set (Pulse 19) compared with the surface temperature predicted for an area far from the arc constriction. The Keidar Boyd model predicts that a temperature measurement made in a location directly under the constriction will have the highest temperature post-pulse cooling curve and that one far from the constriction (i.e. heated only by radiation) will have the lowest temperature cooling curves observed. Any spread between these values may reflect changes in proximity to the actual constriction location. The difference in these measurements suggests that the arc was moving randomly around the propellant face during testing. This is not conclusive proof, as two-dimensional imaging of the

propellant face in the long wavelength IR would be required to assess the constriction location positively on a pulse-to-pulse basis.

The natural vapor pressure of heated Teflon is given by Wentink.[4] The mathematical description of this curve is[1]

$$p_{eq} = p_c e^{-T_c/T_s} \tag{10}$$

where p_{eq} is the equilibrium vapor pressure of Teflon, p_c and T_c are characteristic pressure and temperature values respectively, and T_s is the surface temperature. In this case, $p_c = 1.84 \times 10^{15} N/m^2$ and $T_c = 20{,}815$ K.[1] Combining this estimate of the vapor pressure with the measured surface temperature yields a time-dependent pressure calculation relevant to neutral vapor generation after the pulse. Since the pressure is logarithmically dependent on the surface temperature, small changes in temperature can result in large differences in pressure. Figure 11 shows the timeframe from 26 to 40 μs expanded with post-pulse pressure shown using the temperature from Pulse 20. The pressure uncertainty is based only on the uncertainty in the temperature measurement.

Assuming that after the current pulse each particle liberated is a CF_2 monomer, the average particle mass is 50 AMU. Multiplying this value by Avogadro's number gives an individual molecule mass of 8.3×10^{-23} grams/particle. Using calculations for thermal evaporation common to particle vapor deposition,[21] the surface temperature and vapor pressure can be related to a molecular flux through

$$F = \frac{p_{eq}}{\sqrt{2\pi m k T_s}} \tag{11}$$

where m is the molecule mass, k is the Boltzmann constant, p_{eq} is the equilibrium vapor pressure (from Eqn. 3), and T_s is the surface temperature. This relationship is derived from the Clausius-Clapeyron equation. The molecular flux, F, is the number of molecules liberated from the surface per unit area per unit time. Using the data from Pulse 20 and assuming that the surface temperature measured is representative of the total surface temperature, the molecular flux can be multiplied by the propellant surface area and integrated through time to yield a total molecular evaporation and therefore a total post-pulse mass loss. Figure 12 shows the integration of the mass loss (and molecular evaporation) through time with typical uncertainties.

The total mass lost through post-pulse evaporation using the temperature from Pulse 20 is 1.2±0.6 μg. The average total mass lost per pulse (5.2 μg/pulse) is measured by pulsing 10000 times and measuring thruster mass before and after the pulsing. The post pulse mass loss as a percentage of the total mass lost is 23±11%. This assumes a symmetrical current sheet with exposed Teflon propellant area of 2.13×10^{-5} m^2. Note that the assumption of the measured surface temperature across the propellant face does not necessarily apply due to arc spoking. When the averaged temperature and uncertainties from Pulse 19 are used, the mass loss drops to 0.0176±0.046 μg. This suggests that in areas where the arc is not directly over the propellant face, the expected amount of Teflon liberated from the surface is extremely low for a given pulse. Therefore the total mass likely lost after the pulse is given an upper bound of 1.2±0.6 μg.

5. CONCLUSIONS

This paper described the construction, calibration, and application of HgCdTe photovoltaic detector diagnostic to determine the surface temperature of Teflon propellant during and after the pulse of a microPPT. This diagnostic is shown capable of measuring Teflon surface temperature in real-time after the completion of the current pulse. A theoretical description was developed to predict the detector voltage output. This theory was confirmed by predicting experimental calibration data and then used to estimate a wavelength-dependent emissivity of Teflon in the LWIR. A calibration procedure was created for materials with wavelength dependent emissivity and high transmissive character. This allows application of emissive temperature measurements to materials that until now have been difficult to characterize. Using data from infrared spectroscopy and infrared thermography, a method of estimating the wavelength-dependent emissivity has been developed. To our knowledge these are the first measurements of Teflon surface temperature with infrared thermography as well as the first application of high-speed thermography to discharge physics for analyzing plasma-wall interactions. Although data during the pulse of the micro-PPT is not resolved due to plasma interference, the cooling curve of the propellant is characterized immediately after the pulse. Measurement of the surface temperature of the Teflon propellant during the pulse may be possible if the line transitions in the plasma are sufficiently different from the major emissive structures in the solid Teflon. In this case, a line filter at 8.4 μm over the detector may remove plasma emission sensed through the broadband nature of the detectors used. The possible limitation expected will then be signal-to-noise ratio. Predictions of surface temperature from the Keidar-Boyd model are in good agreement

with experiment. Arc constriction modeling shows a feasible explanation for the range of surface temperatures measured from pulse-to-pulse and is supported by DICAM pictures of anode spotting during operation. For mass loss calculations, an assumption of full surface coverage is used to provide an upper bound of 1.2±0.6 μg which corresponds to 23±11% of the total mass lost.

6. ACKNOWLEDGMENTS

This work is funded by the Air Force Research Laboratory at Edwards AFB, CA and at Kirtland AFB, NM. The research was performed at the Electric Propulsion Laboratory. The authors acknowledge support from ERC Inc. This effort is supported by AFOSR/NA; Dr. Mitat Birkan, program manager.

Figure Captions

Figure 1: Linear HgCdTe detectors shown on a micro-PPT face. The small squares are the detector images and the gray circles are the micro-PPT electrodes. This drawing is to scale.

Figure 2: For calibration, Teflon is sandwiched between a heated copper plate and a back plate. There is no heat source behind the optical access holes.

Figure 3: $1/8^{th}$ inch thick Teflon is sandwiched between copper plates in the calibration jig. Thermocouples are embedded in the sides to approximately the optical viewing location.

Figure 4: Schematic of the (a.) viewable cone for the Plume measurement technique and (b.) target location for the Surface measurement technique.

Figure 5: Estimated a.) non plasma-exposed Teflon emissivity and b.) plasma-exposed Teflon emissivity for 2-12 μm wavelengths.

Figure 6: Calibrations were performed with virgin Teflon and Teflon exposed to micro-PPT plasma conditions. The plasma-exposed data is used for calibration.

Figure 7: Comparison of surface and plume measurements in a micro-PPT. 4.35 J

Figure 8: A test with 14 pulses shows the spread of cooling temperatures measured. Valid data begins after the current pulse ends (26 μs).

Figure 9: Intensified images showing arc behavior at a.) 2.3 J, b.) 5.55 J, and c.) 6.73 J. Capacitance is 0.417 μF.

Figure 10: Measurement of a.) the highest temperature case from the data set shown in Figure 8 with overlying prediction from the Keidar-Boyd model of predicted surface temperature under the arc constriction. b.) shows the lowest cooling temperature from the data set shown in Figure 8 with overlying prediction or surface temperature far from the arc constrition location.

Figure 11: Surface temperature and thruster current for Pulse 20. From 26-40 μs the Teflon vapor pressure is calculated. Data before 20 μs is not valid.

Figure 12: The total number of molecules and mass evaporated based on the surface temperature measurement of Pulse 20.

References

1. R. L. Burton, P. J. Turchi, *J. Prop. Power*, Vol. 14, No. 5, 1998, pp. 716-735.

2. E. L. Antonsen, R. L. Burton, S. F. Engelman, G. G. Spanjers, *Rev. Sci. Instrum.*, **74 (**1), January 2003, pp 88-93.

3. E. L. Antonsen, R. L. Burton, S. F. Engelman, G. G. Spanjers, *Rev. Sci. Instrum.*, **74** (1), March 2003, pp. 1609-1612.

4. Wentink, T. Jr., "High Temperature Behavior of Teflon," AFBMD-TN-59-15 Research Report 55, Avco-Everett Research Laboratory, Everett, MA, July 1959.

5. Zehnder, A. T., Rosakis, A. J., *Journal of the Mechanics and Physics of Solids*, **39** (3), 385-417, 1991.

6. Zehnder, A., T., Rosakis, A. J., "Temperature rise at the rip of dynamically propagating cracks," in: *Experimental Techniques in Fracture III* (Ed. Epstein), Society for Experimental Mechanics, Bethel CT, 125-169.

7. J. Hodowany, G. Rachivandran, A. J. Rosakis, P. Rosakis, *Experimental Mechanics*, **40** (2), 113-123, 2000.

8. Spanjers, G.G., Bromaghim, D.R., Lake, Capt. J., Dulligan, M., White, D., Schilling, J.H., Bushman, S.S., Antonsen, E.L., Burton, R.L., Keidar, M., Boyd, I.D., "AFRL Micro-PPT Development for Small Spacecraft Propulsion," AIAA Paper No. 2002-3974, Indianapolis, IN, July 2002.

9. E. L. Antonsen, R. L. Burton, G. F. Reed, G. G. Spanjers, *J. Prop. Power* **21** (5) Sept/Oct 2005, pp. 877-883.

10. G. G. Spanjers , E. J. Yadlowsky, R. C. Hazelton, J. J. Moschella, *J. Appl. Phys*. **77**, 3657 (1995)

11. R. Arad, K. Tsigutkin, Yu. V. Ralchenko, Y. Maron, *Phys. Plasmas* **7**, 3797 (2000)

12. M. Keidar, I. D. Boyd, E. L. Antonsen, F. S. Gulczinski, G. G. Spanjers, *J. Prop. Power* **20** (6), Nov/Dec 2004, pp 978-984.

13. M. Keidar, I. D. Boyd, E. L. Antonsen, G. G. Spanjers, *J. Prop. Power* **20** (6), Nov/Dec 2004, pp. 961-969.

14. M. Keidar, I. D. Boyd, E. L. Antonsen, R. L. Burton, G. G. Spanjers, *J. Prop. Power* **22** (1), Jan/Feb 2006, pp. 48-55.

15. Fermionics, Simi Valley, CA, www.fermionics.com.

16. Planck, M., *Theory of Heat Radiation*, Dover Publications, New York, 1959.

17. Antonsen, E. L., *Propellant Surface Temperature and Plume Characteristics of Micro-Pulsed Plasma Thrusters*, Ph.D. Dissertation, University of Illinois at Urbana-Champaign, 2004.

18. Holman, J.P., *Heat Transfer 5th Ed*, McGraw-Hill Book Company, 1981.

19. Wertz, J. R., *Mission Geometry; Orbit and Constellation Design and Management*, Microcosm Press, El Segundo, CA, 2001.

20. Book, D. L., *Revised and Enlarged Collection of Plasma Physics Formulas and Data*, NRL Memorandum Report 3332, 1977.

21. Madou, M. J., *Fundamentals of MicroFabrication: The Science of Miniaturization 2nd Ed.*, CRC Press LLC, Boca Raton, FL, 2002.

FIGURES

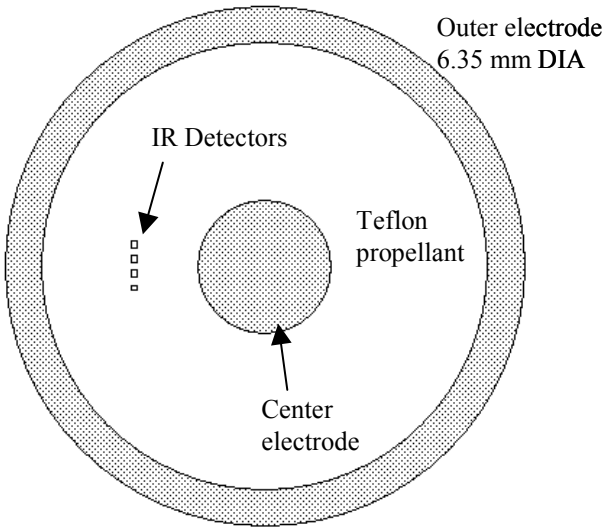

Figure 1. Antonsen et al. "Fast Surface Temperature…"

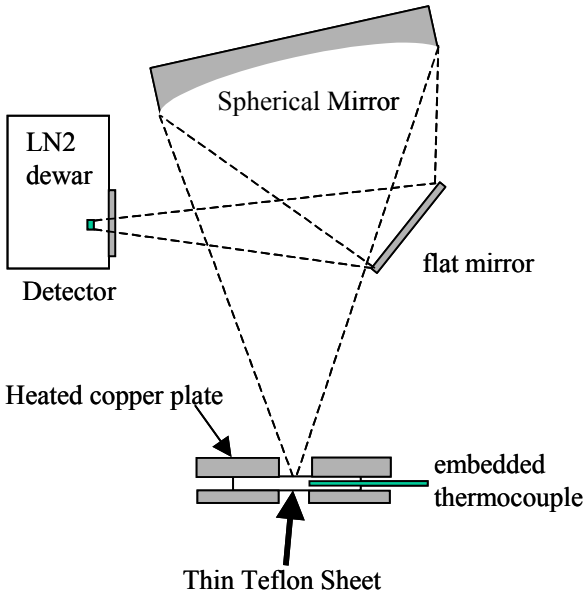

Figure 2: Antonsen et al. "Fast Surface Temperature…"

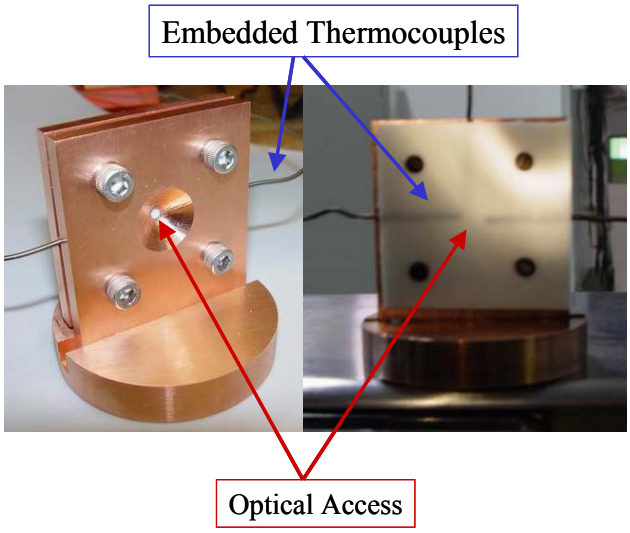

Figure 3: Antonsen et al. “Fast Surface Temperature…”

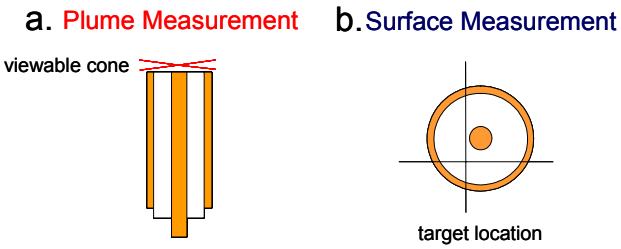

Figure 4: Antonsen et al. "Fast Surface Temperature…"

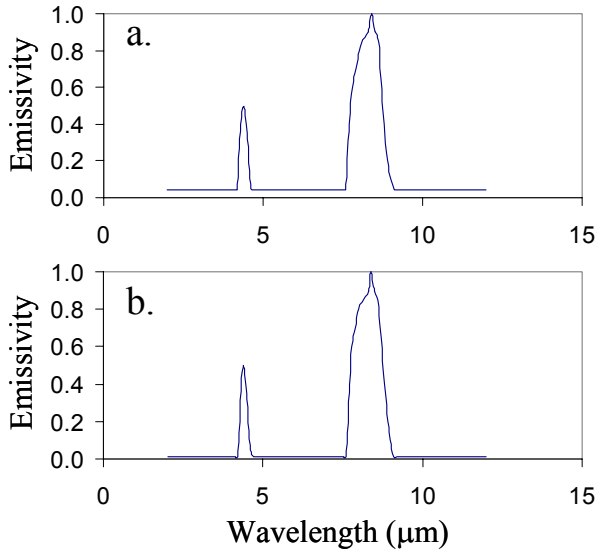

Figure 5: Antonsen et al. "Fast Surface Temperature…"

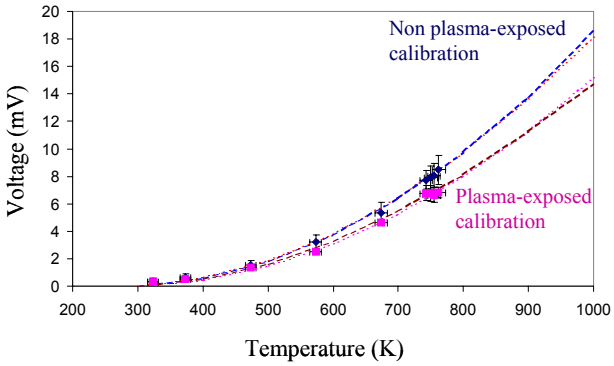

Figure 6: Antonsen et al. "Fast Surface Temperature…"

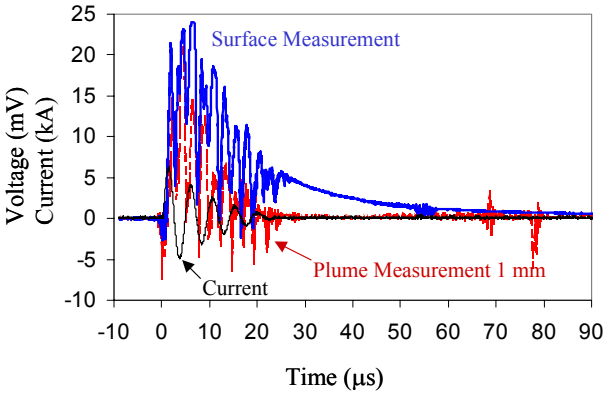

Figure 7: Antonsen et al. "Fast Surface Temperature…"

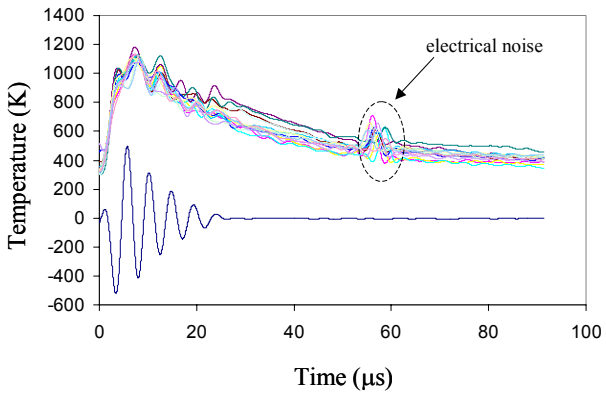

Figure 8: Antonsen et al. "Fast Surface Temperature…"

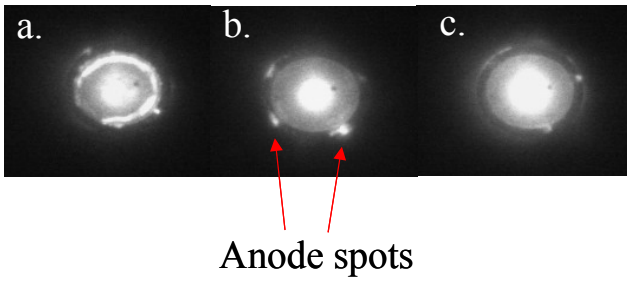

Figure 9: Antonsen et al. "Fast Surface Temperature…"

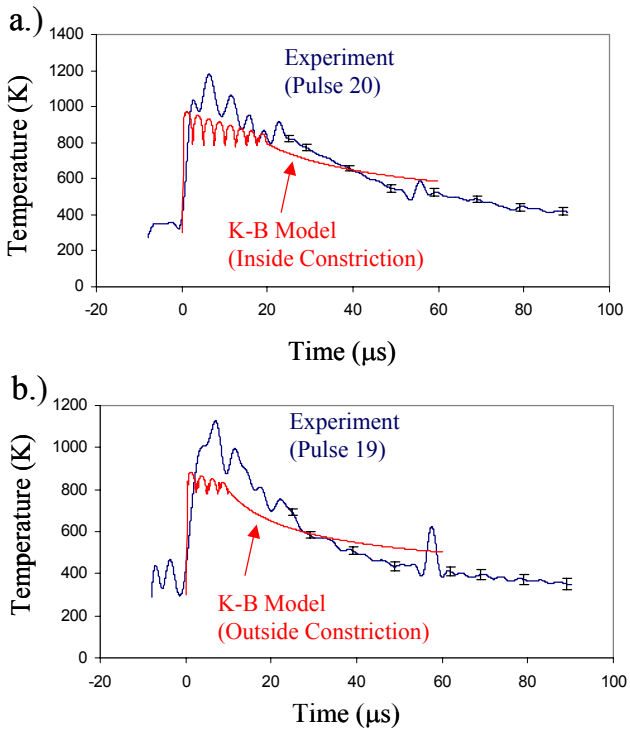

Figure 10: Antonsen et al. "Fast Surface Temperature…"

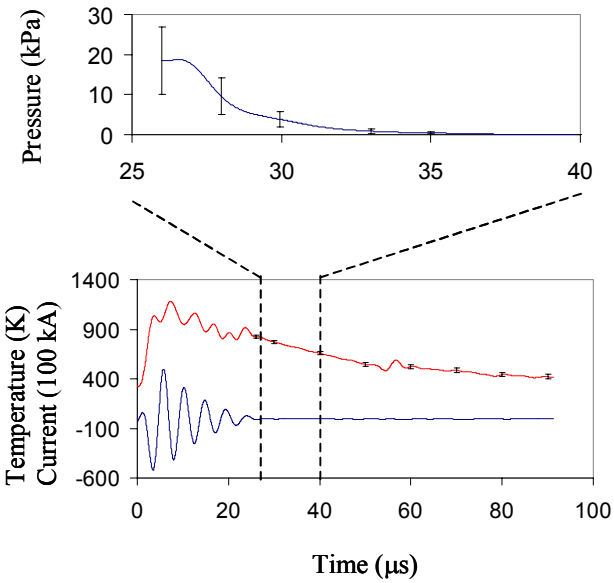

Figure 11: Antonsen et al. "Fast Surface Temperature…"

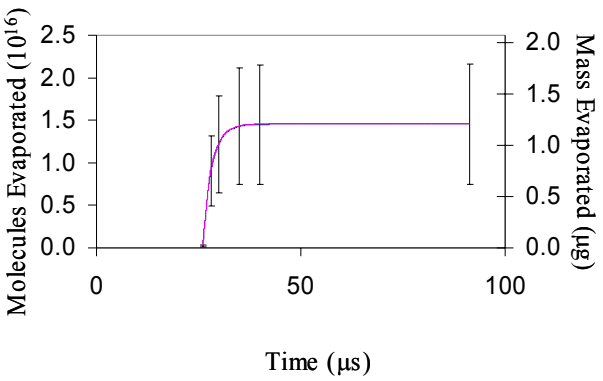

Figure 12: Figure 10: Antonsen et al. "Fast Surface Temperature…"